Quadrupolar Echoes in Solids

I. D. WEISMAN* AND L. H. BENNETT
Institute for Materials Research, National Bureau of Standards, Washington, D. C. 20234
(Received 23 December 1968)

In a classic paper, Solomon showed that the presence of inhomogeneous, first-order quadrupolar interactions leads to the formation of extra "allowed" spin echoes in nuclei for which the spin $I=\frac{5}{2}$. We demonstrate (both theoretically and experimentally) that shifting the rf phase of the second pulse by 90° (in a spin-$\frac{5}{2}$ system) enhances the extra allowed echoes by a factor of almost 5 in amplitude over the unshifted case. Using the density-matrix formulation (and assuming no magnetic inhomogeneities), we have derived, for a 90° phase shift, the amplitude and shape dependence on the second-pulse turning angle of the $\frac{3}{2}\tau$, 2τ, and 3τ echoes. Experimental echo amplitudes and shapes (for both 0° and 90° phase shifts) were obtained, at room temperature, on ^{127}I in a fused sample of KI, and these show good agreement with the calculations. Because of the enhancement, this technique affords a much easier separation of the respective distributions arising from the $\frac{3}{2}\leftrightarrow\frac{5}{2}$ and from the $\frac{1}{2}\leftrightarrow\frac{3}{2}$ satellite transitions than is possible in the unshifted case. Another feature of the phase-shifted case is that, in favorable circumstances, the 3τ echo may be observed although the 2τ echo is obscured by the receiver recovery time. Preliminary data on quadrupole distributions at Al sites in NiAl and $AuAl_2$ intermetallic compounds are presented. Spin-spin relaxation of the satellite transitions is noted. Results expected for systems which have spin values other than $I=\frac{5}{2}$ (both integral and half-integral) are mentioned.

I. INTRODUCTION

NUCLEAR quadrupole interactions are ideal probes for investigating the electronic structure of defects in solids. Strains, dislocations, impurities, variations from exact stoichiometry, and other deviations from the ideal lattice produce distributions of electric field gradients at the various nuclear sites. The method of continuous-wave nuclear magnetic resonance (cw NMR) has been widely and successfully used[1,2] to study these distributions. Usually only indirect information is obtained from these experiments, i.e., the presence of increasingly large quadrupole distributions is inferred from decreases in intensity of the resonance line. In dilute alloys it is sometimes possible to identify the quadrupole interaction associated with impurity atoms at discrete distances.[3] However, as the alloy concentration is increased, the impurities are closer together, and the sharp powder pattern edges at various near-neighbor coordination shells smear out into a broad, weak structure difficult to detect by cw NMR. Another technique that has been useful for dilute alloys is zero-field quadrupole resonance.[4]

The advent of high power, phase coherent, pulsed rf transmitters has opened up a rather exciting chapter in the investigation of the inhomogeneous nuclear quadrupole interactions caused by defects in solids. Solomon,[5] in a classic paper, showed that "quadrupolar" spin echoes could be excited in nuclear spin systems for which the spin $I>\frac{1}{2}$ and, more important, that unique information on the *distribution* of field gradients could be extracted from the echo shapes. He further demonstrated, both theoretically and experimentally, that extra echoes could be elicited in the case of $I=\frac{5}{2}$. The amplitude and character of the echoes depended upon the turning angle of the second pulse in a two-pulse sequence. The method was sufficiently sensitive to measure the distribution of gradients around ^{127}I (spin $\frac{5}{2}$) nuclei in cubic KI under various kinds of strain.

Recently Butterworth[6] pointed out that an inhomogeneous magnetic field (whether externally or internally present) of sufficient strength would suppress the extra echoes in the Solomon case for $I>\frac{3}{2}$ and lead to about a factor of 2 increase in amplitude of the echo at 2τ (τ is the pulse spacing) in all cases where there existed quadrupole interactions. He suggested that combined quadrupolar and magnetic inhomogeneities in metals and alloys could be distinguished from one another in an echo experiment. Preliminary data were presented on Cu-Zn and Cu-Mn. Dowley[7] later exploited this technique in measuring magnetic and quadrupolar interactions both in sponge and small particles of Al. Combined magnetic and quadrupolar interactions in transient NMR experiments have also been discussed by Flett and Richards,[8] who in addition reported results on ^{23}Na in NaCl crystals.

More recently, Bonera and Galimberti,[9] as well as Warren and Norberg,[10] showed that phase shifting the second rf pulse relative to the first in an echo sequence would increase the quadrupolar echo amplitude by about a factor of 3 for $I=\frac{3}{2}$, in the absence of magnetic

* NRC-NBS Postdoctoral Research Associate, 1966–1968.

[1] L. E. Drain, Met. Rev. **119**, 195 (1967), and references therein. Additional references to this kind of work will be noted below.

[2] T. J. Rowland, Phys. Rev. **119**, 900 (1960).

[3] L. E. Drain, J. Phys. **C1**, 1690 (1968).

[4] A. G. Redfield, Phys. Rev. **130**, 589 (1963).

[5] I. Solomon, Phys. Rev. **110**, 61 (1958).

[6] J. Butterworth, Proc. Phys. Soc. (London) **86**, 297 (1965).

[7] M. Dowley, Solid State Commun. **3**, 351 (1965); Phys. Letters **24A**, 428 (1967).

[8] A. M. Flett and J. C. S. Richards, Proc. Phys. Soc. (London) **86**, 171 (1965).

[9] G. Bonera and M. Galimberti, Solid State Commun. **4**, 589 (1966); G. Bonera, A. Avogadro, and F. Borsa, Phys. Rev. **165**, 391 (1968).

[10] W. W. Warren, Jr., and R. E. Norberg, Phys. Rev. **154**, 277 (1967).

inhomogeneities. Bonera and co-workers utilized this technique to measure field gradients at ^{79}Br and ^{81}Br nuclei in NaBr and KBr crystals.[9] Warren and Norberg[10] also capitalized on the 90° phase shift in their study of ^{129}Xe and ^{131}Xe in solid Xe.

In this paper the calculation of the dependence of the echo amplitude and shape on rf phase and turning angle of the second pulse is extended to spin $I=\frac{5}{2}$. Assuming little or no magnetic inhomogeneity, we show that a 90° phase shift nearly doubles the amplitude of the 2τ quadrupolar echo and enhances the extra quadrupolar echoes at $\frac{3}{2}\tau$ and 3τ by a factor of about 5 (compared to the unshifted case). This technique affords a much easier separation of the distributions due to pairs of quadrupolar satellites with *different* transition probabilities (which occur when $I>\frac{3}{2}$) than when there is no rf phase shift between pulses.

In addition, the multiple echoes could (under certain favorable conditions) relax recovery-time restrictions which prevent the observation of any echoes when $\tau\leq\tau_r$. Here τ_r is the recovery time of the detector after an intense rf pulse. As we will show, this could be helpful in studying spin systems in which the recovery times are not too much shorter than the spin-spin relaxation times.

We utilize this new technique to study defects due to strain in an ionic crystal (KI) and defects due to nonstoichiometry in a metallic alloy (NiAl). The latter interests us especially inasmuch as the distribution of electric field gradients is intimately related to the phase stability of the alloy. We do not pursue this relationship in this paper, but expect to do so in the near future. For now, we present preliminary measurements of the echo amplitude of ^{127}I in KI and ^{27}Al in NiAl, and show that these agree quite well with the calculated amplitudes, as a function of the rf phase and turning angle of the second pulse. We also show some results demonstrating the breakdown of the relations when the rf power is reduced.

II. THEORY

A. Density Matrix

The method of handling the calculation of echo amplitude and shape is essentially the treatment developed by Solomon[5] and the notation used in his paper is retained here as much as possible. In the rotating frame the quadrupolar Hamiltonian can be expressed in first order as

$$\mathcal{H}_Q=+a\hbar[I_z^2-\tfrac{1}{3}I(I+1)], \tag{1}$$

where $a=\frac{3}{4}eQV_{zz}/I(2I-1)$, Q is the quadrupole moment, and V_{zz} is the electric field gradient.[11] Five simplifying conditions are assumed:

(a) The applied dc field H_0 is sufficiently large that the quadrupole interaction can be considered a first-order perturbation.

(b) In the rotating frame $\gamma H_1\gg[\langle a^2\rangle_{\rm av}]^{1/2}$. Here γ is the nuclear gyromagnetic ratio, H_1 is the applied rf field, and $[\langle a^2\rangle_{\rm av}]^{1/2}$ represents the rms width of V_{zz}.

(c) Dipolar and other spin-spin interactions can be neglected in comparison with the quadrupolar energy. In general, the treatment of the combined quadrupolar and dipolar systems is extremely difficult[12] and is usually dealt with by only qualitatively considering the dipolar interaction.

(d) The field gradients are axially symmetric.

(e) H_1 is spatially uniform.

We can then immediately proceed to evaluate the echo signal $S(t)$:

$$S(t)=\mathrm{Tr}[\rho(t-\tau)I_+], \tag{2}$$

in which Tr indicates trace and $\rho(t-\tau)$ is the density matrix evaluated at $t-\tau$ after an infinitely narrow 90° rf pulse along the rotating y axis at $t=0$ followed by an infinitely narrow "β" pulse shifted in rf phase by ϕ relative to the first pulse, applied at τ later; β is given by $\gamma H_1\Delta t$, where Δt is the width of the second pulse. More specifically,

$$\rho(t-\tau)=e^{-ia(t-\tau)I_z^2}R_1^{-1}e^{-ia\tau I_z^2}\rho(0)e^{ia\tau I_z^2}\times R_1e^{ia(t-\tau)I_z^2}; \tag{3}$$

$\rho(0)$ is the density matrix immediately after the first pulse at $t=0$ and is given by $I_x=\frac{1}{2}(I_++I_-)$;

$$R_1=e^{i\phi I_z}Re^{-i\phi I_z},$$

and $R=\exp(-i\beta I_y)$. The expression for $S(t)$ becomes

$$\begin{aligned}S(t)&=\sum_{m=-I}^{I-1}\langle m|\rho(t-\tau)I_+|m\rangle\\&=\sum_{m,m',m''}(\langle m|\exp[-ia(t-\tau)I_z^2]R_1^{-1}m''\rangle\langle m''|\exp(-ia\tau I_z^2)\rho(0)|m'\rangle\\&\qquad\times\langle m'|\exp(ia\tau I_z^2)R\exp[ia(t-\tau)I_z^2]I_+|m\rangle)\\&=\sum_{m,m',m''}^{I-1}(\langle m|R^{-1}|m''\rangle\langle m'|R|m+1\rangle\langle m''|\rho(0)|m'\rangle F(m)\exp[i\phi(m'-m''-1)]\\&\qquad\times\exp\{ia[(2m+1)(t-\tau)-(m''^2-m'^2)\tau]\}),\end{aligned} \tag{4}$$

[11] A. Abragam, *The Principles of Nuclear Magnetism* (Clarendon Press, Oxford, England, 1961), p. 231.

[12] P. Mansfield [Phys. Rev. 137, A961 (1965)] has treated combined dipolar and quadrupolar echoes in the case of (a) well-defined quadrupolar satellite transitions, i.e., V_{zz} everywhere the same, and (b) only the central transition is excited.

in which $F(m)=[I(I+1)-m(m+1)]^{1/2}$. Now because of the properties of I_x,

$$\begin{aligned} 2\langle m''|\rho(0)|m'\rangle &= F(m') \quad \text{if} \quad m''-m'=+1 \\ &= F(-m') \quad \text{if} \quad m''-m'=-1. \end{aligned}$$

Also consider that there exists a distribution of field gradients given by $f(\omega_a)$, where $\omega_a=2a$; we make this substitution because $\mathcal{H}_Q$ as defined in Eq. (1) leads to splittings which are $2a$ in magnitude when I is half-integral.

Putting this all together, we obtain from Eq. (4),

$$S(t)=\tfrac{1}{2}\sum_{m,m'=-I}^{I-1}\Big(\langle m|R^{-1}|m'+1\rangle\langle m'|R|m+1\rangle F(m')F(m)\exp(-2i\phi) \times\int_{-\infty}^{+\infty}d\omega_a f(\omega_a)\exp\{i\omega_a[(m+\tfrac{1}{2})(t-\tau)-(2m'+1)\tau]\}\Big)$$

$$+\tfrac{1}{2}\sum_{M=-I,m'=-I+1}^{m=I-1,m'=I}\Big(\langle m|R^{-1}|m'-1\rangle\langle m'|R|m+1\rangle F(-m')F(m) \times\int_{-\infty}^{+\infty}d\omega_a f(\omega_a)\exp\{i\omega_a[(m+\tfrac{1}{2})(t-\tau)-(-2m'+1)\tau]\}\Big). \quad (5)$$

This expression is identical to that obtained by Bonera and Galimberti[9] except that we extend the calculation to $I=\frac{5}{2}$ and look for the functional dependence of the allowed echoes on ϕ and β.

B. 2τ Echo

To obtain the echo at $t=2\tau$ one sets $m=m'$ in the first sum and $m=-m'$ in the second. Taking advantage of the symmetry properties of the R matrices, the signal for the echo at 2τ can be written

$$S(t)_{2\tau}=\tfrac{1}{2}\sum_{m=-I}^{I-1}\{|\langle m|R|-m-1\rangle|^2-|\langle m|R|m+1\rangle|^2\}\exp(2i\phi)[I(I+1)-m(m+1)] \times\int_{-\infty}^{+\infty}d\omega_a f(\omega_a)\exp[ia(m+\tfrac{1}{2})(t-2\tau)]. \quad (6)$$

Evaluating the R-matrix elements[13] for $I=\frac{5}{2}$, one obtains

$$\begin{aligned} S(t)_{2\tau}=&\tfrac{9}{2}\{\cos^2\tfrac{1}{2}\beta(\cos^4\tfrac{1}{2}\beta-6\cos^2\tfrac{1}{2}\beta\sin^2\tfrac{1}{2}\beta+3\sin^4\tfrac{1}{2}\beta)^2-\exp(-2i\phi)\sin^2\tfrac{1}{2}\beta(3\cos^4\tfrac{1}{2}\beta+\sin^4\tfrac{1}{2}\beta-6\cos^2\tfrac{1}{2}\beta\sin^2\tfrac{1}{2}\beta)^2\} \\ &+64\{\cos^2\tfrac{1}{2}\beta\sin^4\tfrac{1}{2}\beta(\tfrac{3}{2}\cos^2\tfrac{1}{2}\beta-\sin^2\tfrac{1}{2}\beta)^2-\exp(-2i\phi)\cos^4\tfrac{1}{2}\beta\sin^2\tfrac{1}{2}\beta(\cos^2\tfrac{1}{2}\beta-\tfrac{3}{2}\sin^2\tfrac{1}{2}\beta)^2\} \\ &\times\int_{-\infty}^{+\infty}d\omega_a f(\omega_a)\cos\omega_a(t-2\tau)+25\{\cos^2\tfrac{1}{2}\beta\sin^8\tfrac{1}{2}\beta-\exp(-2i\phi)\cos^8\tfrac{1}{2}\beta\sin^2\tfrac{1}{2}\beta\} \\ &\times\int_{-\infty}^{+\infty}d\omega_a f(\omega_a)\cos2\omega_a(t-2\tau). \quad (7) \end{aligned}$$

The first bracketed term represents the central-line contribution to the echo and is "time-independent," reflecting the fact that the first-order quadrupole interaction leaves the $-\frac{1}{2}\rightarrow\frac{1}{2}$ transition unchanged. The shape of this signal will be determined by the spin-spin interactions which are presumed to be small and therefore ought to be visible only as a slightly sloped baseline on top of which are superimposed narrower echoes to be described. The second bracket represents the amplitude of the $(\frac{3}{2}\leftrightarrow\frac{1}{2})$ and $(-\frac{1}{2}\leftrightarrow-\frac{3}{2})$ quadrupolar satellite transitions. These terms lead to an echo, the shape of which is determined by the Fourier transform of $f(\omega_a)$. The third bracket represents the amplitude of the echo produced by the outer quadrupolar satellites $(-\frac{5}{2}\leftrightarrow-\frac{3}{2})$ and $(\frac{5}{2}\leftrightarrow\frac{3}{2})$. Notice that the Fourier transform which multiplies this term can be rewritten as

$$\frac{1}{2}\int_{-\infty}^{+\infty}d\omega_a f(\tfrac{1}{2}\omega_a)\cos\omega_a(t-2\tau).$$

[13] M. Tinkham, *Group Theory and Quantum Mechanics* (McGraw-Hill Book Co., New York, 1964), p. 110.

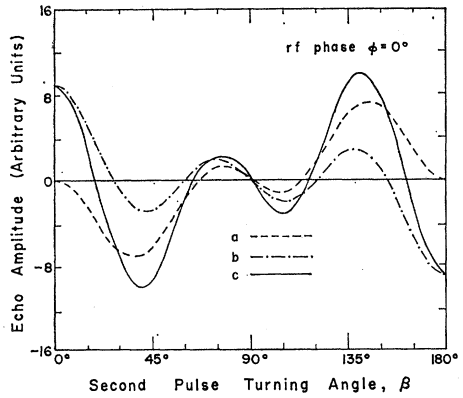

FIG. 1. Plot of the quadrupolar and central transition contributions to the 2τ echo amplitude for $I=\frac{5}{2}$ as a function of the second-pulse turning angle β and rf phase shift ϕ from Eq. (7). The echo amplitudes are shown for the case of no rf phase shift between pulses ($\phi=0°$) and where only an inhomogeneous quadrupolar interaction exists; (a) net quadrupolar contribution, (b) central-transition contribution, and (c) sum of the previous two. In this entire paper, the first pulse is assumed to have a 90° turning angle. An arbitrary normalizing factor has been used for the vertical scale. The same factor is used in Figs. 1–9, so that the echo amplitudes may be directly compared. (Figure 10 has a different normalization factor.)

In other words, as is well known the outer satellites in an $I=\frac{5}{2}$ system have a distribution in frequency which is twice as broad as the inner satellites, leading to an echo at 2τ which is half as wide as the inner satellite echo.

We have plotted the bracketed terms or echo amplitudes discussed above as a function of the turning angle of the second pulse β and for $\phi=0$ (the Solomon case) in Figs. 1 and 2 and for $\phi=90°$ in Figs. 3 and 4. The total echo amplitude both with and without the $(-\frac{1}{2}\leftrightarrow\frac{1}{2})$ contribution is shown in Figs. 1 and 3. It is interesting to note that the application of a sufficiently strong magnetic inhomogeneity $\mathcal{H}_{\text{mag}}=\gamma\hbar bI_z$, where $b\tau>1$, leads to the restriction $m=m'$, so that only the

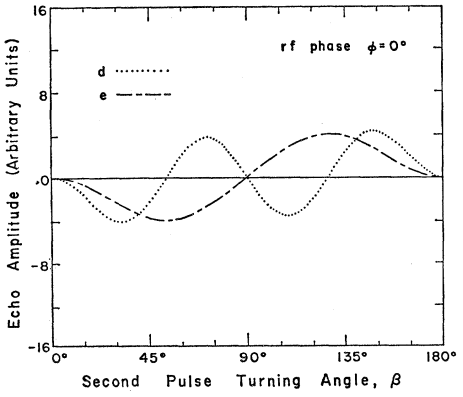

FIG. 2. Plot of the individual quadrupolar satellite contributions to the 2τ echo amplitude when $\phi=0°$. The curves are identified as arising from the following: (d) inner satellite transitions $(-\frac{3}{2}\leftrightarrow-\frac{1}{2})$ and $(\frac{1}{2}\leftrightarrow\frac{3}{2})$, (e) outer satellite transitions $(-\frac{5}{2}\leftrightarrow-\frac{3}{2})$ and $(\frac{3}{2}\leftrightarrow\frac{5}{2})$.

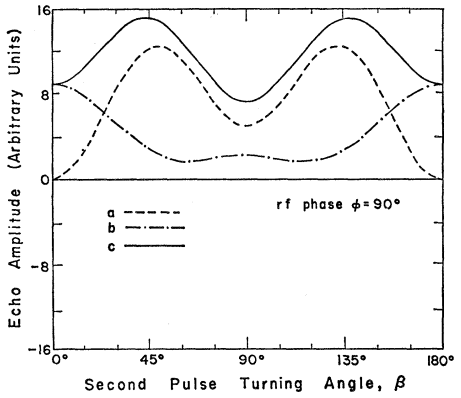

FIG. 3. Plot of various contributions to the 2τ echo amplitude versus β for $\phi=90°$; (a) net quadrupolar contribution, (b) central transition contribution, and (c) total contribution.

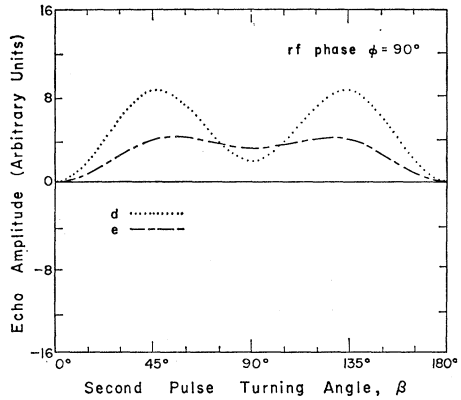

FIG. 4. Plot of the individual quadrupolar satellite contributions to the 2τ echo amplitude when $\phi=90°$. The curves are identified as in Fig. 2.

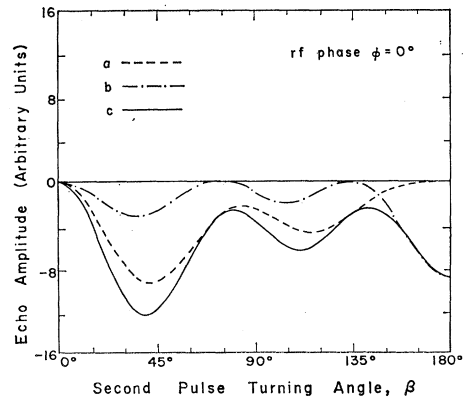

FIG. 5. Plot of the net quadrupolar and central transition contributions to the 2τ echo amplitude versus β when combined inhomogeneous quadrupolar and magnetic interactions are present and where $b\tau>1$ and $\phi=0°$. The curves are labeled as in Fig. 1.

second term in Eq. (6) contributes. (Here b is the z component of the inhomogeneous magnetic field.) Only the echo at $t=2\tau$ then occurs. In this case, phase shifting by 90° simply inverts the echo with no other effect in contrast to the previously mentioned cases.

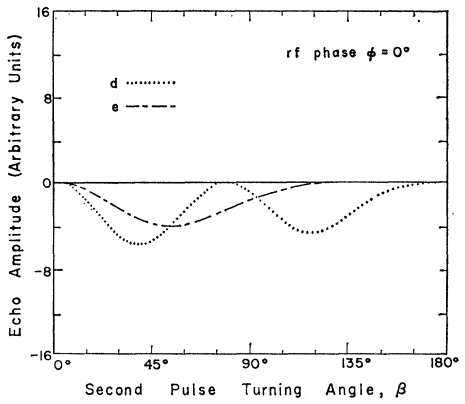

FIG. 6. Plot of the individual quadrupolar satellite contributions to the 2τ echo amplitude versus β for $\phi=0°$ of Fig. 5. The labeling is the same as in Fig. 2.

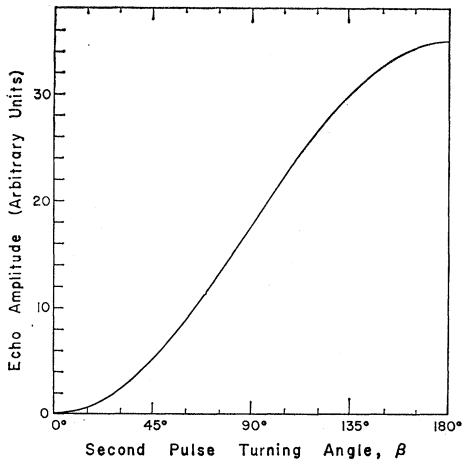

FIG. 7. Plot of the echo amplitude versus β when only an inhomogeneous magnetic field exists.

In Figs. 5 and 6 we have plotted the echo amplitudes for $\phi=0$ when both magnetic and quadrupolar interactions are present and where $b\tau>1$. This is the Butterworth case.[6] It should be noted at this point that if a magnetic inhomogeneity, large compared with the spin-spin interactions, were applied to an $I=\frac{5}{2}$ system and the quadrupolar interaction allowed to vanish, it is straightforward to derive from the density matrix formulation the well-known Hahn echo.[14] The echo signal is given by

$$E(t)=-(35/2)\sin^2\tfrac{1}{2}\beta\int_{-\infty}^{+\infty} db\, f(b)\exp[ib(t-2\tau)].$$

Also in this case the echo appears only at $t=2\tau$. In Fig. 7 we have plotted the amplitude of this echo as a function of β. Such a pattern would be observed, for example, in pure annealed aluminum if a sufficiently large magnetic inhomogeneity were applied.

Comparing the cases of 0° and 90° phase shift, Figs. 1–4, it should be noted that the 90° total satellite echo amplitude (excluding the central transition) reaches its maximum value at about $\beta=48°$ and 132° and is almost a factor of 2 larger than the corresponding $\phi=0°$ maximum echo. In both cases the shape of the echo is determined predominantly by the field gradients through the quadrupole interaction only if the spin-spin decay time is long compared to $2\pi/[\langle a^2\rangle_{\rm av}]^{1/2}$.

C. $\frac{3}{2}\tau$ and 3τ Echoes

Returning to Eq. (5) one notes that other echoes can be formed at $t=[1+(\pm 2m'+1)/(2m+1)]\tau$ when $t\geq\tau$; the plus sign refers to the time dependence in the first sum whereas the minus sign applies to the second sum. In general, for half-integral spins, $(I-\frac{1}{2})\times(I-\frac{3}{2})$ echoes other than that at $t=2\tau$ can be formed. For $I=\frac{5}{2}$ there are two additional echoes, occurring at $t=\frac{3}{2}\tau$ and $t=3\tau$.

The mathematics is straightforward; the signals representing these echoes are

$$S(t)=f_0(\beta)+f_s(\beta)\int_{-\infty}^{+\infty} d\omega_a f(\omega_a)\cos 2\omega_a(t-\tfrac{3}{2}\tau)$$

and (8)

$$S(t)=f_0(\beta)+f_s(\beta)\int_{-\infty}^{+\infty} d\omega_a f(\omega_a)\cos\omega_a(t-3\tau).$$

Here $f_0(\beta)$ is the contribution of the central line and is given as in Eq. (7) by

$$f_0(\beta)=\tfrac{9}{2}\{|\langle-\tfrac{1}{2}|R|-\tfrac{1}{2}\rangle|^2-|\langle-\tfrac{1}{2}|R|\tfrac{1}{2}\rangle|^2e^{-2i\phi}\}$$
$$=\tfrac{9}{2}\{\cos^2\tfrac{1}{2}\beta(\cos^4\tfrac{1}{2}\beta-6\cos^2\tfrac{1}{2}\beta\sin^2\tfrac{1}{2}\beta+3\sin^4\tfrac{1}{2}\beta)^2-e^{-2i\phi}\sin^2\tfrac{1}{2}\beta(3\cos^4\tfrac{1}{2}\beta+\sin^4\tfrac{1}{2}\beta-6\cos^2\tfrac{1}{2}\beta\sin^2\tfrac{1}{2}\beta)^2\}$$

and

$$f_s(\beta)=(\sqrt{40})\{\langle\tfrac{1}{2}|R|\tfrac{5}{2}\rangle\langle\tfrac{3}{2}|R|\tfrac{3}{2}\rangle\exp(-2i\phi)-\langle-\tfrac{1}{2}|R|\tfrac{5}{2}\rangle\langle\tfrac{3}{2}|R|-\tfrac{3}{2}\rangle\}$$
$$=20\{\cos^3\tfrac{1}{2}\beta\sin^2\tfrac{1}{2}\beta(\cos^5\tfrac{1}{2}\beta-4\cos^3\tfrac{1}{2}\beta\sin^2\tfrac{1}{2}\beta)e^{-2i\phi}-\cos^2\tfrac{1}{2}\beta\sin^3\tfrac{1}{2}\beta(\sin^5\tfrac{1}{2}\beta-4\cos^2\tfrac{1}{2}\beta\sin^3\tfrac{1}{2}\beta)\}.$$

The first noteworthy detail here is that these signals (unlike the 2τ echoes) can be unambiguously associated with one pair of quadrupolar transitions. For example, the $\frac{3}{2}\tau$ echo width is determined by the outer satellite distribution (i.e., that due to $-\frac{5}{2}\leftrightarrow-\frac{3}{2}$ and $\frac{5}{2}\leftrightarrow\frac{3}{2}$ transitions), whereas the 3τ echo is a direct measure of the inner satellite distribution ($-\frac{3}{2}\leftrightarrow-\frac{1}{2}$ and $\frac{3}{2}\leftrightarrow\frac{1}{2}$ transitions). While in principle one can analytically separate out this information from the 2τ

[14] E. L. Hahn, Phys. Rev. **80**, 580 (1950).

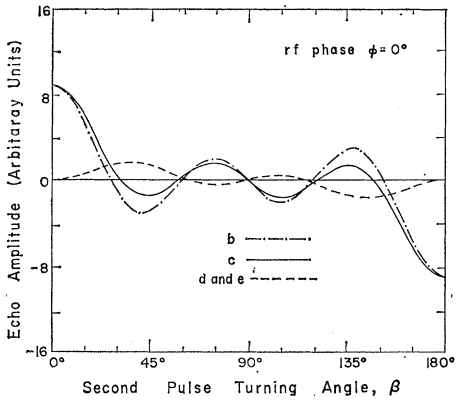

FIG. 8. Plot of the quadrupolar and central transition contributions to the $\frac{3}{2}\tau$ and 3τ echo amplitudes for $I=\frac{5}{2}$ as a function of the second pulse turning angle for $\phi=0°$. The curves in each case represent contributions to the echo from the following: (b) central transition $(-\frac{1}{2}\leftrightarrow\frac{1}{2})$ which is time-independent; (d) inner satellites $(-\frac{3}{2}\leftrightarrow-\frac{1}{2})$, $(\frac{1}{2}\leftrightarrow\frac{3}{2})$ which contribute only to the 3τ echo and; (e) outer satellites $(-\frac{5}{2}\leftrightarrow-\frac{3}{2})$, $(\frac{3}{2}\leftrightarrow\frac{5}{2})$ which contribute only to the $\frac{3}{2}\tau$ echo [note that (d) and (e) have dentical dependences on β in this case]; and (c) sum of (b)+(d) or 3τ echo, or sum of (b)+(e) for $\frac{3}{2}\tau$ echo.

echo using Eq. (7), it is much simpler and more direct to obtain $[\langle\omega_a^2\rangle_{av}]^{1/2}$ from the 3τ or $\frac{3}{2}\tau$ echo shapes.

A second important detail is that the maximum amplitude of these two echoes which occur at $\beta=90°$ when $\phi=90°$ (again ignoring the central transition) is nearly 5 times greater than that attainable when $\phi=0$. In Figs. 8 and 9 we have shown, respectively, the $\frac{3}{2}\tau$ and 3τ echo amplitudes as a function of β with and without the central line contribution for the case of $\phi=0$ in Fig. 8 (Solomon case) and when $\phi=90°$ in Fig. 9. The vertical scale is the same as in Figs. 1–7.

III. EXPERIMENTS

A. Instrumentation

All the spin-echo experiments were performed at 8 MHz and at room temperature on a phase coherent, pulse coherent, crossed-coil spectrometer.[15,16] The power amplifier was capable of producing an rf field in the rotating frame H_1 greater than 160 G with rise and fall times less than 0.25 μsec in a transmitter coil volume of 5 cm^3. The effective sample volume was less than 0.5 cm^3. Crossed coils generally provide a more homogeneous H_1 over the sample volume. The receiver-detector had a recovery time of about 15 μsec. Phase locking the rf pulses to the rf carrier (i.e., pulse coherence) not only helps to reduce receiver recovery time[16] but also eliminates pulse jitter which is particularly annoying when working with narrow ($\leq$1 μsec) pulses. The turning angles of the pulses were measured by comparing the area of the pulse envelope to that of a 90° pulse. When the T_1's were sufficiently short the echo shapes were scanned with a commercial boxcar integrator and plotted out on an X-Y recorder. Otherwise the data were recorded photographically from an oscilloscope display.

B. Sample Preparation

The ^{127}I sample was prepared from powdered KI by heating the material to near its melting temperature where it would fuse and form a solid piece. The object was to increase the density without fracturing the sample so as to improve the NMR signal to noise. Sufficient strains remained in the KI so that quadrupolar echoes were easily observed.

The NiAl intermetallic compound was made in two stages. First, buttons were made in an arc furnace with a water-cooled hearth by melting together 99.995 Ni and 99.99 Al. These buttons were then remelted in an induction furnace in a recrystallized triangle RR aluminum oxide crucible *in vacuo*. Metallographic examination revealed no second phase. The NMR sample was prepared by hand filing the button. The powder was then sealed in an evacuated quartz tube and annealed for 1 h at 1000°C.[17] Another sample was prepared from the same button by grinding in a shaker mill, but was not annealed. Results obtained on it were not significantly different from those observed on the annealed sample although no attempt was made to calibrate NMR intensities. The stoichiometry was not measured in this experiment. However, a more comprehensive investigation is planned in which specific stoichiometry as determined by chemical and other means will be correlated with cw NMR intensities as well as quadrupolar echo shapes.

C. Results on KI

In order to verify Eqs. (7) and (8), echoes were observed on ^{127}I (spin $\frac{5}{2}$) in KI at room temperature

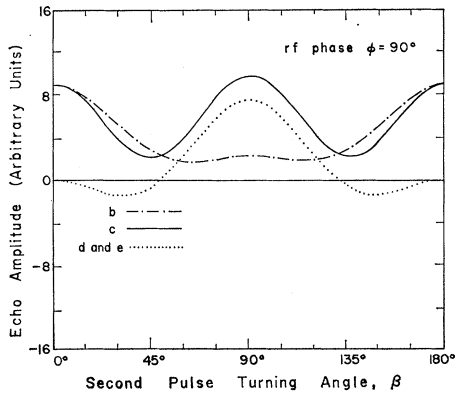

FIG. 9. Same as Fig. 8, except $\phi=90°$.

[15] The rf and pulse circuitry of the transmitter were taken from a design by John Brewer of Argonne National Laboratory. Dr. R. M. Cotts supervised the construction of the receiver from a design by W. G. Clark [Rev. Sci. Instr. **35**, 316 (1964)] during a sabbatical at the National Bureau of Standards.

[16] The clamp circuitry was designed by J. J. Spokas, Rev. Sci. Instr. **36**, 1436 (1965).

[17] G. W. West, Phil. Mag. **9**, 979 (1964); **15**, 855 (1967).

using an H_1 of about 160 G. In many respects ^{127}I in KI is ideal for this experiment. In our sample the free induction decay from the central line had a Gaussian shape with a width at half-maximum of 0.570 msec corresponding to an absorption half-width at half-maximum of about 0.41 kHz. On the other hand, the half-widths of the quadrupolar echoes were no larger than 13 μsec so that (a) the echoes could be observed over a time interval much smaller than the spin-spin decay time and (b) τ could be large enough to minimize interference from the quadrupolar portion of the free induction decay immediately following the second pulse. Also the quadrupolar interactions were easily saturated by the H_1 available. In addition the sample had a T_1 of about 16 msec so that it was convenient to use a boxcar integrator to improve signal to noise. The echo widths were found to be independent of H_1 for $H_1 \geq 45$ G. First, the amplitude of the echo at 2τ was measured as a function of β where $\phi = 90°$, and these results are plotted in Figs. 10(a) and 10(b) where the central-line contribution has been subtracted out. In Fig. 10(c) we have shown the measured amplitude of the $\frac{3}{2}\tau$ echo versus β on the same scale again with $\phi = 90°$, and with the central-line contribution subtracted out. The amplitude of the 3τ echo was found to be the same as that of the $\frac{3}{2}\tau$ echo for all β.

Figure 11 shows ^{127}I echoes for various pulse sequences which are indicated by $90°-\tau-\beta_\phi$ where $\tau \simeq 110$ μsec. All sequences except in Fig. 11(f) were made with $H_1 = 80$ G. Two interesting effects are to be pointed out here. (a) The $\frac{3}{2}\tau$ and 3τ echoes which are barely visible in Fig. 11(g), (the $90-\tau-40_0$ sequence should maximize these echoes for the $\phi = 0°$ case) are enhanced by almost a factor of 5 in Fig. 11(c) where $\beta = \phi = 90°$ as was indicated earlier. Note that the echo at 2τ in Figs. 11(g) and 11(h) is inverted in phase with respect to the 2τ echo in Fig. 11(c) and that "quadrupolar" amplitudes are referred to the base line signal which is

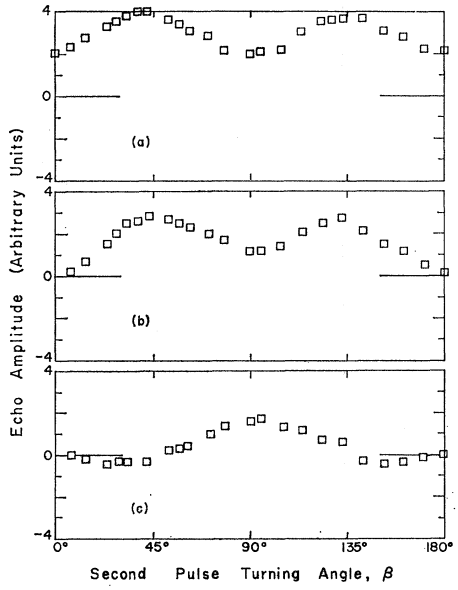

FIG. 10. Plot of the experimentally measured amplitude of the echoes at $\frac{3}{2}\tau$ and 2τ of ^{127}I in a solid polycrystalline sample of KI as a function of β. The 2τ echo amplitude is shown in (a) whereas in (b) the total 2τ echo amplitude minus the central-transition contribution is plotted. The $\frac{3}{2}\tau$ echo amplitude from which the central-transition contribution has been subtracted is shown in (c). The data were taken at 8 MHz using an rf field H_1 of about 160 G. Here τ was about 100 μsec. Note that $\phi = 90°$.

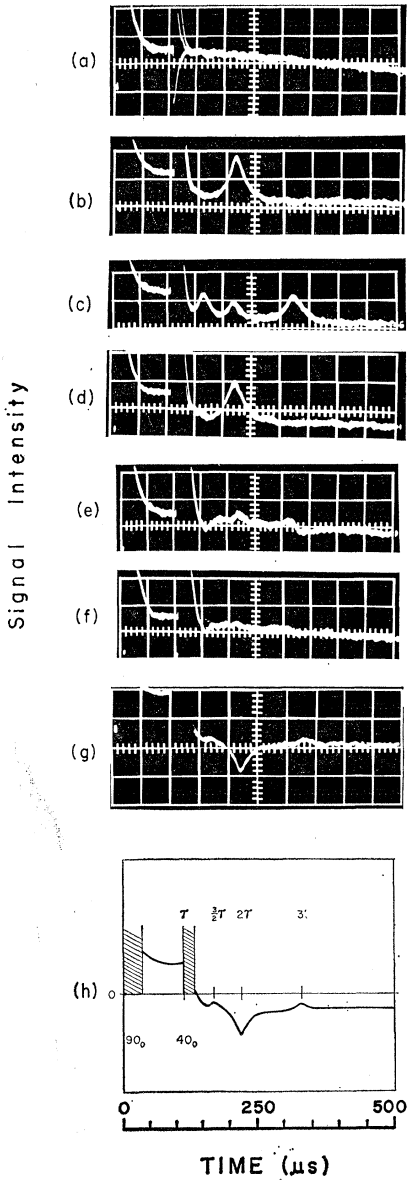

FIG. 11. Oscilloscope traces of ^{127}I echoes in a solid polycrystalline sample of KI for the following pulse sequences: (a) $90-\tau-5_{90}$, (b) $90-\tau-45_{90}$, (c) $90-\tau-90_{90}$, (d) $90-\tau-135_{90}$, (e) $90-\tau-180_{90}$, (f) $90-\tau-180_{90}$, (g) $90-\tau-40_0$, and (h) schematic drawing of (g) which may be helpful in deciphering the photographs. The full length of each oscilloscope trace is 500 μsec. The rf field was 80 G except in (f) where it was raised to 160 G. (g) and (h) should be compared to (c) to see the effect of phase shifting on the $\frac{3}{2}\tau$ and 3τ echoes. The factor of 5 should be apparent in comparing the extra echo amplitudes (see text for details).

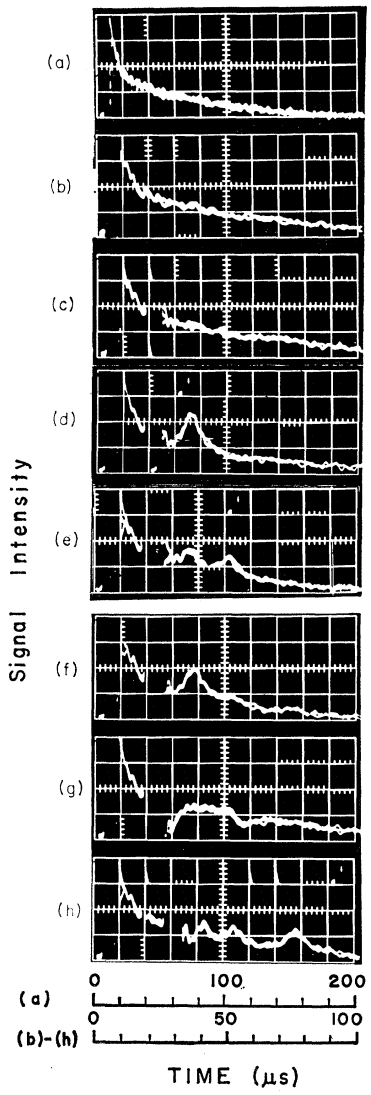

FIG. 12. Oscilloscope traces of quadrupolar echoes observed on ^{27}Al in intermetallic NiAl. The pulse sequences are as follows: (a) One 90° pulse, free induction decay; the total trace measures 200 μsec. (b) One 90° pulse, free induction decay; the total trace is 100 μsec. (c) $90°-\tau-5°_{90}°$, $\tau\sim16$ μsec; (d) $90-\tau-45_{90}$; (e) $90-\tau-90_{90}$; (f) $90-\tau-135_{90}$; (g) $90-\tau-180_{90}$; and (h) $90-\tau-90_{90}$ with a larger τ, $\tau\sim25$ μsec. Note the $\frac{3}{2}\tau$ echo.

the decay of the $(-\frac{1}{2}\leftrightarrow\frac{1}{2})$ signal. (b) While the echo widths were found to be independent of H_1, it was found that the $90-\tau-180_{90}$ sequence, Fig. 11(e), retained a small amount of quadrupolar echo contrary to Fig. 3. When H_1 was raised to 160 G the structure was attenuated. This structure consists of vestiges of the allowed echoes. However, in common with the "forbidden" echoes discussed by Solomon,[5] it is the result of the fact that the ratio $H_1/[\langle a^2\rangle_{\rm av}]^{1/2}$ is not infinitely large. We found that the $\frac{3}{2}\tau$ and 3τ echoes were exponential rather than Gaussian with half-widths of, respectively, 5.8±0.5 and 12.5±0.5 μsec. (The signs represent estimated uncertainties both here and elsewhere in the paper.) These numbers correspond to Lorentzian distribution functions, $\frac{1}{2}f(\frac{1}{2}\omega_a)$ and $f(\omega_a)$, with half-widths at half-maxima of, respectively, 19±2 and 9±1 kHz for the outer and inner satellites. We note here that the effects of the inhomogeneous H_1 would be to smear out the relatively sharp minima and maxima of the quadrupolar echo amplitude as a function of β, but no smearing was observed in our crossed coil probe.

D. Preliminary Results on NiAl

In extending the quadrupolar echo technique to metals we chose ^{27}Al in NiAl because of the relatively long spin-spin decay time and because it had a spin of $\frac{5}{2}$ and a relatively strong signal. Although this intermetallic is of the cesium chloride structure it has a wide range of stoichiometry near the equiatomic composition over which there are departures from cubic symmetry.[17] The Al resonance in these compounds has been well characterized as a function of stoichiometry, using cw methods, by West'[17] and by Seitchik and Walmsley,[18] but the actual range of the quadrupolar interaction was not measured; this is a task for which the pulse method is ideal.

Solid echoes were observed at $\frac{3}{2}\tau$, 2τ, and 3τ in annealed samples of NiAl (see Sec. III B) at 8 MHz and at 298 K. The echo amplitudes were in agreement with those predicted by Figs. 1–4, 8, and 9. An H_1 in excess of 160 G was used and appeared sufficient to saturate the spectrum within experimental error. Oscilloscope traces of the ^{27}Al (in NiAl) echoes as well as the free induction decay are shown in Fig. 12. In the sequences displayed, τ was too short for the $\frac{3}{2}\tau$ echo to be observable but has been increased in Fig. 12(h) so as to make this echo more obvious. Figure 12(g), in common with the I in KI, shows quadrupolar structure on a $90-\tau-180_{90}$ sequence. In this case, the structure could very well be the "forbidden" echo at $\frac{5}{2}\tau$ expected when $\gamma H_1/[\langle a^2\rangle_{\rm av}]^{1/2}\gg1$ is not completely satisfied. As can be seen in Figs. 12(a) and 12(b), the Al free induction decay has considerable amounts of quadrupole structure immediately after the rf pulse which makes it somewhat difficult to obtain the width of that part due only to the central line. Signal-to-noise consderations aggravated by a rather long T_1 ($T_1\sim80$ msec) precluded an accurate extrapolation to extract the central-line decay time. However, it appears that the decay time calculated from either the data of West[17] or Seitchik *et al.*[18] is consistent with our results. A crude estimate of the ratio of the 2τ echo amplitude extrapolated to $\tau=0$ to that of the central-line free induction decay extrapolated to $t=0$ suggests that all Al sites are experiencing strong field gradients. Our measured half-widths, $T_{1/2}$ at half-echo maxima are as follows. $\frac{3}{2}\tau$ echo: $T_{1/2}=2.0\pm0.8$ μsec; 2τ echo: $T_{1/2}=3.5\pm0.5$ μsec; 3τ echo: $T_{1/2}=4\pm0.5$ μsec. The 2τ and 3τ

[18] J. A. Seitchik and R. H. Walmsley, Phys. Rev. **131**, 1473 (1963).

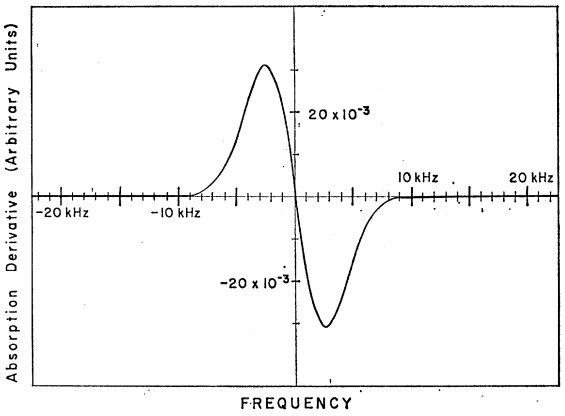

FIG. 13. Theoretical line-shape derivative plotted for ^{27}Al in NiAl assuming that the central line is Gaussian with a peak-to-peak width of 5.0 kHz and that the quadrupolar distributions are Lorentzian. The central linewidth was taken from the data of Ref. 18 and the satellite information was extracted from our experimental echo shapes. An arbitrary normalization factor has been used for the vertical scale. The same factor is used in Figs. 13–15, so that the absorption derivatives may be directly compared.

measurements were made for $\tau\sim16$ μsec whereas the $\frac{3}{2}\tau$ echo was measured at $\tau=25$ μsec. No changes in the former echo shapes were noted for $\tau=25$ μsec within the experimental error. We could not distinguish between an exponential and Gaussian decay of the $\frac{3}{2}\tau$ and 3τ echoes. If the decay were Gaussian the distribution function $f(\omega_a)$ for the inner quadrupolar satellites would be Gaussian with a half-width at half-maximum of 55±7 kHz, whereas the outer satellites would have a Gaussian distribution with a half-width at half-maximum equal to 110±44 kHz. Accordingly, if the echo shape were exponential the distributions $f(\omega_a)$ and $\frac{1}{2}f(\frac{1}{2}\omega_a)$ would be Lorentzian with half-widths at half-maxima of, respectively, 28±3 and 55±22 kHz.

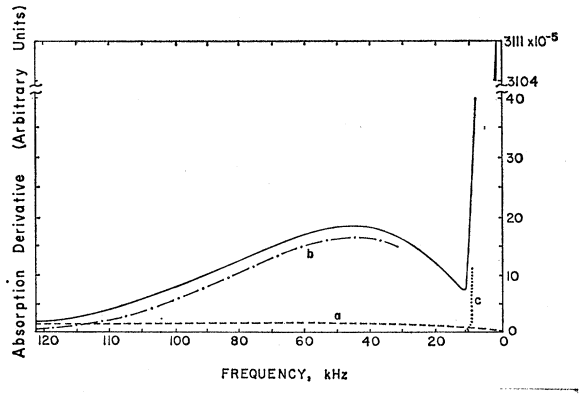

FIG. 14. Total theoretical line-shape derivatives plotted for ^{27}Al in NiAl assuming Gaussian shapes for both satellite and central-line distributions. Only the low-frequency portion of the total line shape is shown; the high-frequency portion is identical except opposite in sign. The vertical scale has been broken at the top in order to show the relative height of the central-line peak. In addition, outer satellites, inner satellites, and central-line distributions are given by the curves marked *a*, *b*, and *c*, respectively.

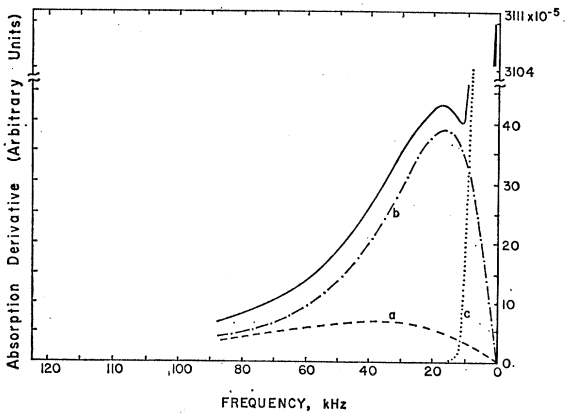

FIG. 15. Total theoretical line-shape derivatives plotted for ^{27}Al in NiAl assuming Lorentzian satellite distributions and a Gaussian central line. Only the low-frequency portion of the total line shape is shown; the high-frequency portion is identical except opposite in sign. The vertical scale has been broken at the top in order to show the relative height of the central-line peak. In addition, the outer satellite, inner satellite, and central-line distributions are given by the curves marked *a*, *b*, and *c*, respectively.

In order to understand how these echoes contribute to the observed cw spectrum we have assumed a total distribution function

$$f_T(\omega)=\frac{9}{35}f_c(\omega)+\frac{16}{35}f_1(\omega)+\frac{10}{35}f_2(\omega), \qquad (9)$$

for the ^{27}Al line in NiAl, where $f_c(\omega)$ is the normalized Gaussian representing the central-line absorption, and where $f_1(\omega)=f(\omega_a)$ and $f_2(\omega)=\frac{1}{2}f(\frac{1}{2}\omega_a)$ are, respectively, the individually normalized inner and outer quadrupolar satellite absorption functions. In practice, one observes the derivative of $f_T(\omega)$ in a cw experiment and we have accordingly plotted out $df_T(\omega)/d\omega=(1/2\pi)df(2\pi\nu)/d\nu$ in Figs. 13–15 (ν is in frequency units). The peak-to-peak width for the central line was taken from the data of Seitchik *et al.*[18] ($\delta\nu=5.0$ kHz) whereas the peak-to-peak widths for the satellite lines were obtained from our echo widths. For the latter, one uses the following relationship:

$$\text{Gaussian: } \Delta\omega_{pp}/2=(2\ln 2)^{1/2}/T_{1/2},$$

$$\text{Lorentz: } \Delta\omega_{pp}/2=1/\sqrt{3}T_2=(\ln 2)/\sqrt{3}T_{1/2}.$$

Here $\Delta\omega_{pp}$ is the peak-to-peak derivative width and $T_{1/2}$ is the appropriate echo half-width at half-maximum. For example, $T_{1/2}$ for $\Delta\omega_{pp}$ of $f_1(\omega)$ is measured from the 3τ echo and $T_{1/2}$ corresponding to $\Delta\omega_{pp}$ of $f_2(\omega)$ is measured from the $\frac{3}{2}\tau$ echo. Figure 13 shows the full absorption derivative which comes from $df(2\pi\nu)/d\nu$ under the assumption of a Gaussian central line and Lorentzian satellites. The satellite structure is barely visible in the tails of the central line. To illustrate this in more detail we have magnified the vertical scale in Fig. 15 and shown only half of the total line. The curves marked *a*, *b*, and *c* are, respectively,

$(10/35)f_2(\omega)$, $(16/35)f_1(\omega)$, and $(9/35)f_c(\omega)$ (outer satellites, inner satellites, and central line). Figure 14 repeats Fig. 15 except that satellite distributions are Gaussian. In both Figs. 14 and 15 the vertical scale has been broken at the top in order to show the central-line derivative peak for comparison. The long tails are the first obvious differentiation of the satellite contributions from the central-line shape. This is not surprising since Rowland[2] had observed similar structure by cw NMR on ^{63}Cu in CuGe alloys. However, another feature is the structure which appears in Fig. 15 between -10 and -17 kHz and in Fig. 14 between -10 and -30 kHz. The amplitude of this structure, due primarily to the inner satellites, is very weak compared to the central-line peak, i.e., of the order of 0.1–0.3%. The outer satellite distribution is so broad and so weak that no structure attributable to it can be observed even on our magnified scale.

On the other hand, there were systems in which we expected quadrupolar echoes to be absent such as the Al at the cubic site in $AuAl_2$ and in pure annealed Al metal. The former appears to have a very high degree of crystallographic order, where as the latter has obvious cubic symmetry. A signal was observed from Al nuclei in both systems and, as expected, did not appear to be quadrupolar in nature. Unlike the cases of I in KI and Al in NiAl, no extra echoes could be seen at $\frac{3}{2}\tau$ or 3τ, and the signal did not change shape appreciably with variation of β.

IV. OTHER REMARKS

A. Satellite Relaxation Times

In studying both the ^{127}I and ^{27}Al resonances in KI and NiAl, respectively, it was noticed that the quadrupolar echoes decayed more slowly (with no obvious change in shape) than the central-line component as a function of τ, i.e., T_2 for satellites $> T_2$ of central transition. This effect has been observed before.[8] It reflects the fact that two neighboring spins will, in general, experience different field gradients especially if the quadrupolar interactions are much larger than any spin-spin energy. The mutual spin-flip terms of the spin-spin Hamiltonian are inhibited because energy cannot be conserved. This suggests that, even when τ becomes of the order of the spin-spin decay time of the central line, the echo shape still measures the satellite distributions directly (provided that the echo width is much narrower than the central-line spin-spin decay time). However, a more specific statement in this regard must await a comprehensive analytical treatment of the combined quadrupolar and dipolar echoes where all transitions are saturated by the rf field.

B. Recovery Time

In certain cases where instrument recovery time limits the minimum τ for observation of a 2τ echo it may be possible to utilize the echo at 3τ to relax this restriction. To see this, consider the criterion for observation of an echo occurring at time $n\tau$ in the presence of instrument recovery time τ_r, $n\tau > \tau + \tau_r$ or $\tau > \tau_r/(n-1)$. Observability of a 3τ echo requires only that $\tau > \frac{1}{2}\tau_r$, where as it must be larger than τ_r for a 2τ echo. To capitalize on this apparent reduction in recovery time, the echoes must be fairly narrow compared to τ (so as to avoid interfering with one another).

C. Other Spin Values

Although we deal explicitly with $I=\frac{5}{2}$ in this paper, many of the results are immediately applicable to other spin values. We noted earlier that, for half-integral spin I, there were $(I-\frac{1}{2})(I-\frac{3}{2})$ extra echoes, in addition to the one at 2τ. The analogous expression for integral spin is $I(I-1)$. For example, for $I=\frac{7}{2}$, there will be six such echoes, at $\frac{4}{3}\tau$, $5\tau/3$, $\frac{3}{2}\tau$, $\frac{5}{2}\tau$, 3τ and 4τ; the outer, middle, and inner satellites individually determine the shapes of, respectively, the first, second, and third pair of echoes denoted above. When $I=\frac{9}{2}$ there will be 12 echoes, with each of four sets of satellite transitions governing the shape of three echoes. No difficulty would be anticipated in observing the echoes beyond $t=2\tau$. One might expect considerable overlap of signals which occur for $t<2\tau$, unless τ is sufficiently large compared with the echo width. However, unique information can be obtained on these systems even with the above limitations.

V. CONCLUSION

In this paper we have shown that phase shifting the second pulse of spin echo sequence by 90° in the $I=\frac{5}{2}$ case enhances the extra allowed echoes by a factor of almost 5. The $\frac{3}{2} \leftrightarrow \frac{5}{2}$ and $\frac{1}{2} \leftrightarrow \frac{3}{2}$ satellite transitions are separately measurable. It is apparent that while cw NMR experiments can measure significant inhomogeneous quadrupolar interactions in solids with some difficulty, the transient quadrupolar echo technique can accomplish this task more directly and far more quantitatively. In fact, cw spectra of NiAl had revealed no satellite structure. The reconstruction of cw line shape using the quadrupolar echoes demonstrates clearly the difficulties in attempting direct observation of quadrupolar structure. Extension to higher spin systems is obvious but possibly more complex experimentally because of the large number of echoes for $t<2\tau$.

ACKNOWLEDGMENTS

We express our sincere thanks to Dr. J. J. Spokas and J. Brewer of Argonne National Laboratory for their help in the design and construction of the high-powered transmitter. We thank V. M. Johnson for technical assistance.

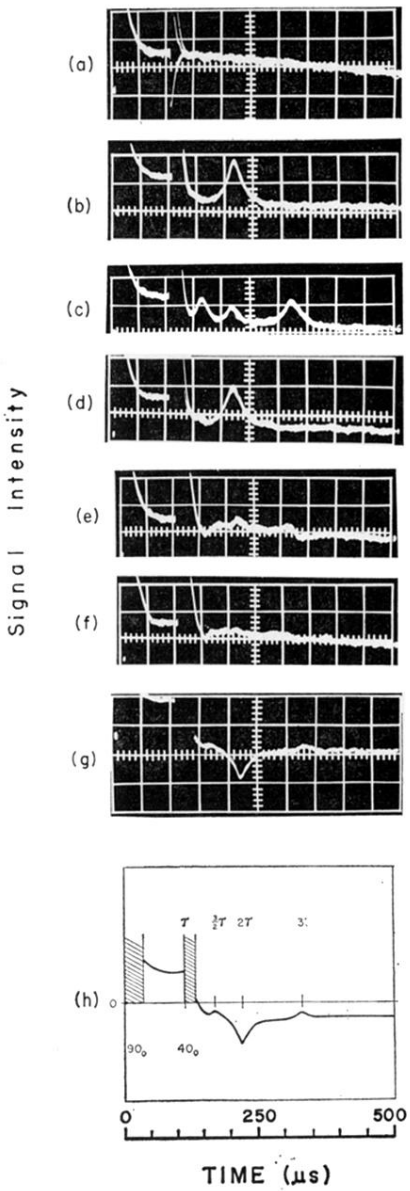

FIG. 11. Oscilloscope traces of ^{127}I echoes in a solid polycrystalline sample of KI for the following pulse sequences: (a) $90-\tau-5_{90}$, (b) $90-\tau-45_{90}$, (c) $90-\tau-90_{90}$, (d) $90-\tau-135_{90}$, (e) $90-\tau-180_{90}$, (f) $90-\tau-180_{90}$, (g) $90-\tau-40_0$, and (h) schematic drawing of (g) which may be helpful in deciphering the photographs. The full length of each oscilloscope trace is 500 μsec. The rf field was 80 G except in (f) where it was raised to 160 G. (g) and (h) should be compared to (c) to see the effect of phase shifting on the $\frac{3}{2}\tau$ and 3τ echoes. The factor of 5 should be apparent in comparing the extra echo amplitudes (see text for details).

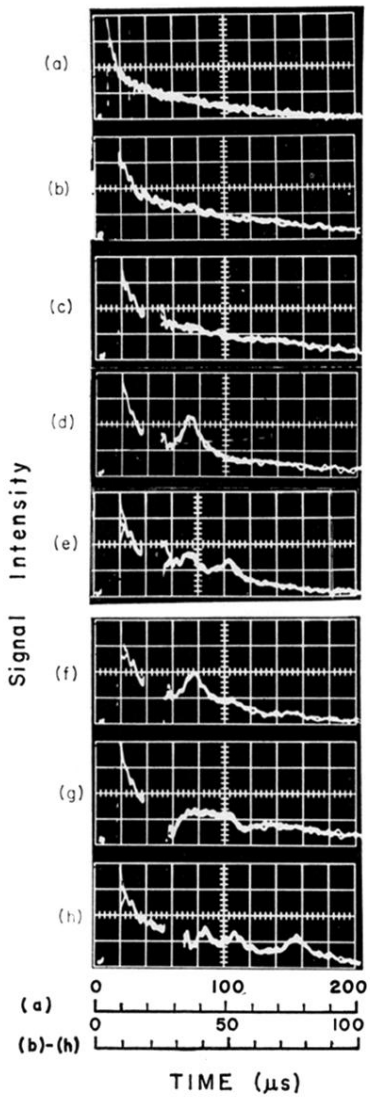

FIG. 12. Oscilloscope traces of quadrupolar echoes observed on ^{27}Al in intermetallic NiAl. The pulse sequences are as follows: (a) One 90° pulse, free induction decay; the total trace measures 200 μsec. (b) One 90° pulse, free induction decay; the total trace is 100 μsec. (c) $90°-\tau-5°_{90}°$, $\tau\sim16$ μsec; (d) $90-\tau-45_{90}$; (e) $90-\tau-90_{90}$; (f) $90-\tau-135_{90}$; (g) $90-\tau-180_{90}$; and (h) $90-\tau-90_{90}$ with a larger τ, $\tau\sim25$ μsec. Note the $\frac{3}{2}\tau$ echo.